

---

# GRAPH CONCEPT BOTTLENECK MODELS

---

**Haotian Xu**

Department of Applied Mathematics and Statistics  
Stony Brook University  
Stony Brook, NY 11794  
haotian.xu@stonybrook.edu

**Tsui-Wei Weng**

Hacıoğlu Data Science Institute  
University of California, San Diego  
La Jolla, CA 92093  
lweng@ucsd.edu

**Lam M. Nguyen**

Thomas J. Watson Research Center  
IBM Research  
Yorktown Heights, NY 10598  
lamnguyen.mltd@ibm.com

**Tengfei Ma**

Department of Biomedical Informatics  
Stony Brook University  
Stony Brook, NY 11794  
tengfei.ma@stonybrookmedicine.edu

## ABSTRACT

Concept Bottleneck Models (CBMs) provide explicit interpretations for deep neural networks through concepts and allow intervention with concepts to adjust final predictions. Existing CBMs assume concepts are conditionally independent given labels and isolated from each other, ignoring the hidden relationships among concepts. However, the set of concepts in CBMs often has an intrinsic structure where concepts are generally correlated: changing one concept will inherently impact its related concepts. To mitigate this limitation, we propose **Graph CBMs**: a new variant of CBM that facilitates concept relationships by constructing latent concept graphs, which can be combined with CBMs to enhance model performance while retaining their interpretability. Our experiment results on real-world image classification tasks demonstrate Graph CBMs offer the following benefits: (1) superior in image classification tasks while providing more concept structure information for interpretability; (2) able to utilize latent concept graphs for more effective interventions; and (3) robust in performance across different training and architecture settings.

## 1 Introduction

Deep neural networks have demonstrated remarkable performance and efficiency across a wide range of tasks in Computer Vision [1, 2, 3], Natural Language Processing [4, 5, 6, 7], and Graph Learning [8, 9, 10]. Despite their success, these models are often considered black boxes due to their lack of interpretability. In safety-critical domains such as medical applications, this opacity raises concerns, as there is a growing demand for transparent and reliable decision-making processes.

To address this issue, Concept Bottleneck Models (CBMs) [11] have been introduced to enhance interpretability by mapping hidden representations to a human-understandable concept space. In CBMs, each neuron in the bottleneck layer corresponds to a specific concept with an associated confidence score. Unlike end-to-end models that map raw inputs (e.g., pixel values) directly to output labels, CBMs make predictions based on the activation scores in the concept space. This formulation enables human intervention on the concept activation vector to alter predictions without modifying model parameters.

However, existing CBMs overlook a key aspect: *the correlations among concepts*. In reality, certain concepts often co-occur, e.g., “fur” and “whiskers” typically suggest the presence of “tail” or “paws,” while “wings” and “beak” imply “feathers.” Such patterns are well-established in cognitive science; for instance, [12] show that visual neurons respond more strongly when related concepts appear together, suggesting the brain encodes concept relevance implicitly. Yet recent CBM approaches [13, 14, 15] fail to model these natural correlations. Ignoring such relationships undermines model trustworthiness, as co-varying concepts can provide critical contextual cues to aid human understanding [16, 17].

This omission weakens interpretability and trust, especially in domains like healthcare, where co-occurring symptoms provide crucial context. For instance, during diagnosis, our model can suggest likely symptoms and their interrelations, while allowing doctors to intervene and make the final decision.

Motivated by these insights, we introduce **Graph CBMs**, a framework designed to uncover intrinsic correlations among concepts through a learnable graph structure and complement to existing CBMs with enhanced performance and interpretability. We hypothesize the existence of a unified, input-independent concept graph that encodes prior semantic knowledge, where individual input samples activate only a subset of relevant concepts. We represent this graph structure using a Graph Neural Network (GNN), and learn it via self-supervised contrastive learning. In our approach, the subgraph of activated concepts for an input image is treated as an augmented view, forming positive samples in the contrastive loss. This encourages the learned graph to capture semantically grounded relations and enables the graph to be integrated as a plug-in module across various CBM variants.

**Our key contributions are summarized as follows:**

- We propose **Graph CBMs**, which incorporate a learnable concept graph to model interactions among concepts, thereby enhancing both prediction performance and interpretability.
- We develop a self-supervised learning framework that automatically constructs latent concept graphs. Empirical results demonstrate its effectiveness on both classification and intervention (on average 1%~2% improvement across 8 datasets).
- Our approach shows strong generalization across settings, with or without concept annotations, and works robustly across different backbones. Moreover, Graph CBMs remain effective even under concept interventions.

## 2 Related Work

**Concept Bottleneck Models (CBMs)** aim to improve interpretability by first predicting human-interpretable concepts before classifying inputs [11]. Subsequent work has expanded this idea: CBMs model concept embeddings [13, 14], address limited concept sets and predictor expressiveness [18], and apply energy-based models to joint input-concept-label tuples [19]. However, these models typically require expensive concept annotations. To reduce this burden, recent efforts leverage large pretrained models to automate concept discovery [20, 21]. For instance, [21] selects diverse and discriminative concepts via submodular optimization, while PCBM [15] minimizes reliance on concept labels by training only the final layer. Label-Free CBMs [20] further automate the process by incorporating sparse prediction layers to enhance interpretability and accuracy. Recent work also improves concept selection [22]. In contrast to these approaches, which often treat concepts independently, our method explicitly models their interactions via latent graph structures, and can be integrated with existing CBMs.

**Graph Structure Learning (GSL)** aims to infer useful graphs from raw data. Early methods emerged in signal processing [23] and probabilistic graphical models [24]. In the deep learning era, GSL is often integrated with graph neural networks (GNNs) [25, 26, 27, 28, 29]. For example, NRI [26] learns latent interaction graphs in dynamic systems using latent variables, while [25] treats GSL as a bi-level optimization problem over discrete edge distributions. Recent advances also explore contrastive learning for hypergraphs [30]. Our approach aligns with this line by learning a deterministic latent graph end-to-end through contrastive supervision, tailored to model concept relationships.

## 3 Graph Concept Bottleneck Models

Graph CBMs aim to introduce latent graph structures into the concept space. Learning such latent topologies, also known as graph structure learning has proven beneficial across domains, including time series [27], physical systems [26], and computer vision [28], even when explicit graph structures already exist [25]. In human vision, interactions among fine-grained concepts also enhance recognition [16, 17, 12]. We extend this idea to CBMs by modeling concepts as nodes and their interactions as edges, forming a concept graph that captures relational structure. *This graph not only supports prediction but also offers interpretability by revealing how concept interactions influence decisions.*

### 3.1 Preliminaries

**Concept Bottleneck Models (CBMs):** Given a set of images  $V = v_1, v_2, \dots, v_n$  and a predefined set of concepts  $T = t_1, t_2, \dots, t_k$ , each image  $v_i$  is associated with a label  $y_i \in \mathcal{Y}$ . A CBM consists of two components: a mapping  $f_1$  from the image space to the concept score space, and a mapping  $f_2$  from the concept score space to the label space. The image is first projected into the concept space via  $c_i = f_1(v_i; T) \in \mathbb{R}^k$ , producing concept scores. These scores are

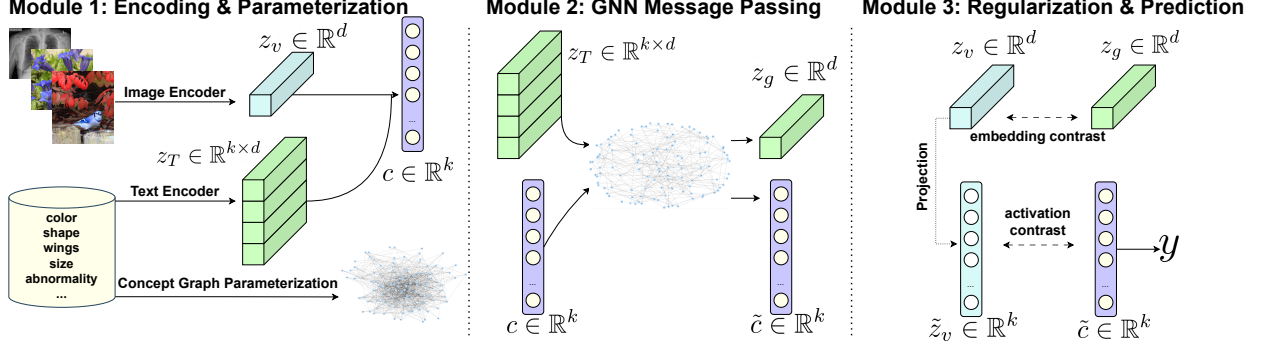


Figure 1: Overview of Graph CBM. ① Extract embeddings via pretrained encoders and initialize the graph structure. ② Update the concept embeddings and concept activations through message passing. ③ Use different granularity contrastive losses to qualify the latent graph and make final predictions.

used to predict the final label:  $\hat{y}_i = f_2(c_i)$ . Each element  $c_i^j$  ( $1 \leq j \leq k$ ) reflects the relevance between image  $v_i$  and concept  $t_j$ .

**Our Setting:** Given an image  $v_i$  and a concept set  $T$ , our goal is to identify a subset of activated concepts that both describe and help classify the image effectively. Following the label-free CBM setting [20], we assume access to pretrained multimodal encoders:  $E_v : V \rightarrow \mathbb{R}^d$  and  $E_t : T \rightarrow \mathbb{R}^d$ , which embed images and concepts into a shared latent space. We denote the concept embedding matrix as  $z_T = E_t(T) \in \mathbb{R}^{k \times d}$ . For each image  $v_i$ , the initial concept score vector is computed via the dot product:  $c_i = z_T z_{v_i} \in \mathbb{R}^k$ , where  $z_{v_i} = E_v(v_i)$ . If ground-truth concept annotations are available, concept scores can alternatively be obtained via a learnable MLP:  $c_i = \text{MLP}(z_{v_i})$ .

We define the latent concept graph as  $G = (V, \mathcal{A})$ , where the node set  $V$  corresponds to the concepts, and the adjacency matrix  $\mathcal{A}$  encodes structural relations among them. In Figure 1, we show our procedures for learning the latent concept and will explain it in more detail in the following sections.

### 3.2 Module 1: Encoding and Parameterization

Module 1 prepares the inputs for our Graph-CBM model and consists of two components: (1) encoding images and concepts using pretrained encoders, and (2) parameterizing the initial latent concept graph, which will be refined in later stages.

#### 3.2.1 Encoding Images and Concepts

There are two primary CBM training settings: the *label-free* and *concept-supervised* paradigms. In the label-free setting, concept annotations are unavailable, and concept sets must be defined heuristically at the dataset or instance level [21, 20].

In both settings, images are passed through a pretrained vision encoder to obtain image embeddings. For label-free CBMs, the concept descriptions are also processed through a pretrained language encoder to extract their embeddings. Importantly, both encoders remain necessarily frozen during CBM training to avoid converting the pipeline into a fully end-to-end model, thereby preserving the interpretability of the concept space.

#### 3.2.2 Parameterizing the Initial Graph

The purpose of the latent concept graph is to model the underlying relationships among concepts. Since the concept set is defined at the dataset level, the same latent graph structure  $\mathcal{A}$  is shared across all data instances. To enable finer control and interpretability, we decompose the graph node representation into two components: the semantic embedding set  $V_{\text{emb}} = \{z_{T,i}\}$  and the activation vector  $V_{\text{act}} = c_i$ . Thus, the full graph is denoted as  $G_i = (V_{\text{emb}}, V_{\text{act}}, \mathcal{A})$ .  $\mathcal{A}$  will be the same across instances, whereas  $V_{\text{emb}}$  and  $V_{\text{act}}$  will become instance-dependent during training.

$V_{\text{emb}} \in \mathbb{R}^{k \times d}$  captures the intrinsic meaning of each concept node, while  $V_{\text{act}} \in \mathbb{R}^{k \times 1}$  reflects the extent to which each concept is activated per instance. The adjacency matrix  $\mathcal{A}$  encodes initial structural relations between concept nodes. We initialize  $\mathcal{A}$  either by computing similarities among node embeddings or randomly. Empirically, we find that random initialization achieves comparable performance, so we adopt it for simplicity.

Although  $\mathcal{A}$  is shared across instances in a dataset, the distinction brought by  $V_{\text{act}}$  will trigger different nodes in the latent concept graph (we consider a concept node being activated if the corresponding entry value in  $V_{\text{act}}$  is positive), resulting input-dependent graph structure in end.

### 3.3 Module 2: GNN Message Passing

With the latent concept graph, we can derive better representations of images through concept node embeddings and activations in the graph. To enhance the expressive capacity of structure learning, we adopt a multi-layer approach, where each layer is associated with its own learnable adjacency matrix. Specifically, we define the graph at layer  $l$  as  $G_i^l = (V_{\text{emb}}^{l-1}, V_{\text{act}}^{l-1}, \mathcal{A}^l)$ , where  $l$  denotes the layer index. The final latent concept graph is constructed as the union of edge sets across all layers, i.e.,  $\bigcup_l \mathcal{A}^l$ . In practice, we use 3 layers for structure learning.

At each layer  $l$ , we follow a standard message passing framework [8] to aggregate neighborhood information and propagate it to the concept nodes. Since concept nodes at layer  $l$  are characterized by both embeddings ( $V_{\text{emb}}^{l-1}$ ) and activations ( $V_{\text{act}}^{l-1}$ ), we perform two distinct message passing steps at each layer.

We apply the renormalization trick introduced in [8] to the adjacency matrix:  $\text{Renormalize}(\mathcal{A}^l) = \tilde{D}^{-\frac{1}{2}} \tilde{\mathcal{A}}^l \tilde{D}^{-\frac{1}{2}}$ , where  $\tilde{\mathcal{A}}^l = \mathcal{A}^l + I$ ,  $\tilde{D}_{ii} = \sum_j \tilde{\mathcal{A}}_{ij}^l$ . Here,  $I$  denotes the identity matrix, and  $\tilde{D}$  is the degree matrix of  $\tilde{\mathcal{A}}^l$ .

The update equations for embeddings and activations at layer  $l$  are given by:

$$V_{\text{emb}}^l = \sigma \left( \tilde{D}^{-\frac{1}{2}} \tilde{\mathcal{A}}^l \tilde{D}^{-\frac{1}{2}} [V_{\text{act}}^{l-1} \odot V_{\text{emb}}^{l-1}] \right), \quad V_{\text{act}}^l = \sigma \left( \tilde{D}^{-\frac{1}{2}} \tilde{\mathcal{A}}^l \tilde{D}^{-\frac{1}{2}} V_{\text{act}}^{l-1} \right) \quad (1)$$

Here,  $\odot$  denotes element-wise multiplication. The product  $V_{\text{act}}^{l-1} \odot V_{\text{emb}}^{l-1}$  captures the degree to which each concept node is activated in the latent concept graph at layer  $l$ .  $\sigma(\cdot)$  is a non-linear activation function.

### 3.4 Module 3: Regularization & Prediction

To capture intrinsic interactions within the concept space, concept graphs must remain independent of label supervision, as labels can introduce spurious correlations that obscure genuine concept dependencies. We address this by using contrastive learning, treating each image and its activated concept graph as a positive pair. This encourages the model to learn label-agnostic structures while also providing supervision in label-free settings.

After message passing, we apply a mean pooling to extract a graph-level representation for each input image:  $z_{g_i} = \text{MeanPooling}(V_{\text{emb}}^m) \in \mathbb{R}^d$ , where  $m$  is the number of layers. As previously discussed, the concept graph acts as an augmentation technique for input images. Under the assumption of intrinsic concept relationships, we introduce a contrastive regularization term based on the normalized temperature-scaled cross-entropy loss (NT-Xent) [31]. Moreover, relying solely on the embedding-wise contrastive loss yields suboptimal performance (see Tables 3 and 4). Inspired by [32, 33, 34, 35], we design a second contrastive loss at a different granularity to further regularize the updated concept scores  $\tilde{c}_i$ . We treat  $\tilde{c}_i = V_{\text{act}}^m$  as the positive pair for image  $v_i$  in  $\mathbb{R}^k$  (the concept space). We project  $z_{v_i}$  into the same space using an MLP layer  $f_3: \mathbb{R}^d \rightarrow \mathbb{R}^k$ , yielding  $\tilde{z}_{v_i} = f_3(z_{v_i}; \phi)$  as the anchor point in the concept space.

$$\mathcal{L}_{\text{emb}} = -\log \left( \frac{\sum_{i=1}^n \frac{e^{\text{sim}(z_{v_i}, z_{g_i})/\tau}}{\sum_{j=1, j \neq i}^n e^{\text{sim}(z_{v_i}, z_{g_j})/\tau}} \right), \quad \mathcal{L}_{\text{act}} = -\log \left( \frac{\sum_{i=1}^n \frac{e^{\text{sim}(\tilde{z}_{v_i}, \tilde{c}_i)/\tau}}{\sum_{j=1, j \neq i}^n e^{\text{sim}(\tilde{z}_{v_i}, \tilde{c}_j)/\tau}} \right), \quad (2)$$

where  $\text{sim}(\cdot, \cdot)$  denotes the cosine similarity, and  $\tau$  is a temperature hyperparameter (set to  $\tau = 0.3$  in our experiments). In each mini-batch, the positive pair consists of the image embedding  $z_{v_i}$  (or  $\tilde{z}_{v_i}$ ) and its corresponding concept graph embedding  $z_{g_i}$  (or  $\tilde{c}_i$ ), while the negative pairs are the graph embeddings of all other images.

The two contrastive losses operate at different layers and regulate the latent graph structure from complementary perspectives. Specifically,  $\mathcal{L}_{\text{emb}}$  enforces alignment and uniformity between the image and graph-level embeddings, while  $\mathcal{L}_{\text{act}}$  encourages concept activation vectors to serve as effective hidden representations of the input images [36]. Combining both with a prediction loss and a sparsity regularization term, the final loss becomes:

$$\mathcal{L} = \text{CE}(\hat{y}_i, y_i) + \alpha(\mathcal{L}_{\text{emb}} + \mathcal{L}_{\text{act}}) + \beta \ell_1(\mathcal{A}), \quad (3)$$

where  $\text{CE}(\cdot, \cdot)$  is the cross-entropy loss,  $\ell_1(\cdot)$  denotes L1 regularization, and  $\alpha, \beta$  are weighting hyperparameters. The prediction  $\hat{y}_i$  is computed by passing  $\tilde{c}_i$  through another MLP  $f_2: \mathbb{R}^k \rightarrow \mathcal{Y}$ , i.e.,  $\hat{y}_i = f_2(\tilde{c}_i)$ .



The above formulation is primarily designed for the *label-free* setting. When concept supervision is available, the model directly learns concept representations from ground-truth annotations. In such cases, we no longer require a language encoder to obtain concept embeddings, and the contrastive loss reduces to  $\mathcal{L}_{act}$ , alongside a sparsity regularization term. The final loss function in the concept-supervised setting becomes:

$$\mathcal{L} = \text{CE}(\hat{y}_i, y_i) + \text{BCE}(\hat{c}_i, \tilde{c}_i) + \alpha \mathcal{L}_{act} + \beta \ell_1(\mathcal{A}), \quad (4)$$

where  $\text{BCE}(\cdot, \cdot)$  is the binary cross-entropy loss. Since concept annotations provide structural cues, the BCE loss guides the latent graph to align with these ground-truth relationships. Simultaneously,  $\mathcal{L}_{act}$  regularizes the graph by treating  $\tilde{c}_i$  as a meaningful latent representation of image  $v_i$ . Together, they enable the model to learn a high-quality latent graph structure.

Base experiments	CUB	Flower102	HAM10000	Cifar-10	Cifar100
LF-CBM	73.90% ( $\pm 0.28\%$ )	84.77% ( $\pm 0.59\%$ )	66.76% ( $\pm 0.43\%$ )	86.40% ( $\pm 0.10\%$ )	65.16% ( $\pm 0.14\%$ )
Graph-(LF-CBM)	<b>75.59%</b> ( $\pm 0.18\%$ )	<b>86.00%</b> ( $\pm 0.98\%$ )	<b>67.47%</b> ( $\pm 0.61\%$ )	<b>86.54%</b> ( $\pm 0.15\%$ )	<b>65.96%</b> ( $\pm 0.16\%$ )
PCBM	73.84% ( $\pm 0.16\%$ )	79.01% ( $\pm 1.19\%$ )	77.61% ( $\pm 0.60\%$ )	95.71% ( $\pm 0.07\%$ )	80.02% ( $\pm 0.39\%$ )
Graph-PCBM	<b>77.14%</b> ( $\pm 0.40\%$ )	<b>89.25%</b> ( $\pm 0.69\%$ )	<b>78.50%</b> ( $\pm 0.52\%$ )	<b>95.95%</b> ( $\pm 0.09\%$ )	<b>80.86%</b> ( $\pm 0.26\%$ )

Table 1: **Graph CBM can better capture image information.** We report the mean and standard deviation from 10 random runs.

## 4 Experiments & Results

### 4.1 Setup

**Datasets:** For evaluating Graph CBMs, we choose various real-world datasets ranging from common objects to dermoscopic images. We introduce 1) common objects: CUB [37], Flower102 [38], AwA2 [39], and CIFAR [40]; and 2) medical domains: HAM10000 [41] and ChestXpert [42]. Dataset details can be found in appendix A.

Since many datasets do not contain concept annotations, we will use LLMs to generate and filter the concept set for each dataset. In CUB and CIFAR datasets, we use the same concept sets provided by [20]. Furthermore, we found that concepts can be redundant and noisy in CIFAR datasets; thus, we apply the submodular filtering algorithm [21] to reduce the number of concepts in (G-)PCBM experiments. For Flower and HAM10000, we use the concept candidates in [21].

**Baseline:** We choose the state-of-the-art CBM models that do not need concept annotations during training, i.e., LF-CBM [20] and Post-hoc CBMs (PCBM) [15]. For multi-modality encoders, we choose the standard CLIP [43]. For a fair comparison with Label-free CBMs, we use CLIP(ViT-B/16) and CLIP(RN50) as the image encoder and the backbone (ResNet-18 trained on CUB from imgcls mob as the backbone for CUB). In the concept-supervised setting, standard CBMs [11] and CEMs [13] serve as our baseline, and we still use CLIP(ViT-B/16) to extract features on CUB (112 concepts) and AwA2 (85 concepts) dataset. For ChestXpert (11 concepts), we use BioViL [44] as the image encoder, as BioViL is pre-trained on large X-ray datasets. We use the Adam optimizer and cosine scheduler during training. More configuration details and efficiency concerns are offered in Appendix B.

### 4.2 Latent Graphs Enhance Model Performance

**Graph-LF-CBM and Graph-PCBM can substantially outperform their counterparts without graphs under label-free settings.** Observing the solid enhancement in Table 1 of having a latent concept graph across different datasets, we can conclude the effectiveness of our proposed method. To better understand the benefit of having a latent concept graph, we draw T-SNE plots for  $c_i$  ( $\tilde{c}_i$ ) in Figure 5 Appendix E, showing that models with latent concept graphs can better cluster concept activations to corresponding label groups. In Table 10 Appendix G, our method surpasses the baseline on large-scale datasets, which further validates the effectiveness of using latent concept graphs.

**Graph CBMs can generalize their improvements to concept-supervised settings.** In Table 2, adding the latent graph can increase the label prediction performance for all the datasets from different domains, and match or even surpass the baseline’s capability on concept prediction. It is important to note that the latent graph is primarily designed to **leverage interactions among concepts** to improve label prediction and enable more effective interventions, rather than directly

optimize concept-level predictions. Furthermore, our models still demonstrate notable improvements in some cases, particularly, G-CEM not only boosts label prediction accuracy over standard CEM but also narrows the gap in concept prediction performance compared to CBM-based approaches.

Method	CUB		AwA2		ChestXpert	
	Label	Concept	Label	Concept	Label	Concept
CBM	78.45%	<b>70.40%</b>	95.24%	<b>97.48%</b>	66.40%	<b>83.41%</b>
Graph-CBM	<b>80.03%</b>	68.33%	<b>95.34%</b>	97.05%	<b>66.82%</b>	83.20%
CEM	80.86%	61.34%	95.21%	98.16%	66.73%	77.93%
Graph-CEM	<b>81.11%</b>	<b>61.53%</b>	<b>95.49%</b>	<b>98.62%</b>	<b>66.93%</b>	<b>78.27%</b>

Table 2: Comparison between label prediction and concept prediction. We report the average accuracy (for label prediction) and roc-auc (for concept prediction) from 10 random seed experiments.

### 4.3 Comparison with SOTAs

In Figure 2, we compare our proposed method with state-of-the-art models to demonstrate the effectiveness of constructing a latent concept graph. We evaluate our method under both *label-free* and *concept-supervised* settings using the CUB dataset, a common benchmark for concept-based modeling. For the label-free setting, we include additional strong baselines such as BotCL [45], CDM [46], LaBo [21], and Res-CBM [47]. For the concept-supervised setting, we compare against ProbCBM [14], HardAR [18], E-CBM [19], and S-CBM [48].

Under the label-free setting, LaBo and Res-CBM perform well but rely on large concept sets (e.g., 10,000 for CUB). In contrast, our G-PCBM achieves higher accuracy using only 200 concepts, fewer training epochs, and a comparable backbone (e.g., ViT-L/14 improves G-PCBM from 77.1% to 82.3%). For other reference, [22] reports 63.9% with the same setup. This demonstrates the efficiency and effectiveness of leveraging latent graphs in CBMs.

In the concept-supervised setting, our models, G-CBM and G-CEM, perform competitively with the best current methods. HardAR and E-CBM both aim to model latent concept correlations but follow fundamentally different approaches. HardAR focuses on autoregressively generating concept scores, assuming sequential dependencies. Our method, by contrast, employs graph-based modeling, which is inherently **permutation-invariant** and better suited to capturing rich, non-linear concept interactions. Furthermore, our latent graphs can seamlessly plug into HardAR’s framework to further enhance its relational reasoning through message passing.

Compared to E-CBM, which encodes concept dependencies implicitly via energy-based modeling, our approach offers **explicit** graph structures that are easier to visualize and interpret. This transparency is especially valuable for downstream tasks such as intervention (see Section 4.4). The learned graph not only improves model performance during training but also enables more effective post-hoc analysis and decision manipulation.

Importantly, our method is **orthogonal** to existing CBM designs and can be **flexibly integrated** into a variety of architectures. To support this claim, we present a case study with CDM [46] in Appendix H, showing how latent graphs can complement other CBM variants. Moreover, unlike models such as HardAR, E-CBM, or S-CBM that require datasets with explicit concept annotations, our latent graph framework is **versatile** and can be applied in both concept-supervised and label-free CBM settings, broadening its applicability across domains.

### 4.4 Intervention Dynamics

A core advantage of CBMs lies in their **intervenability**: allowing users to adjust concept activations to correct false predictions and improve trust. Beyond enhancing label prediction post-training, we evaluate whether latent graphs further strengthen CBMs during concept interventions. *Notably, the benefit of incorporating latent graphs becomes more pronounced in this setting, as relational cues help guide more effective interventions.* Following the UCP policy [49], we select relevant concepts and apply a simple *Lazy Intervention* strategy (Appendix D) to modify activation values.

**In both label-free and concept-supervised settings, incorporating a latent graph improves intervention performance.** As defined in Equation 1, the message passing mechanism allows changes in the intervened activation vector  $c_i$  to propagate to neighboring concepts via the latent graph, amplifying the effect to calculate the final  $\tilde{c}_i$ . Thus, models with graphs implicitly intervene more broadly, leading to more robust corrections, as shown in Figure 3 A.

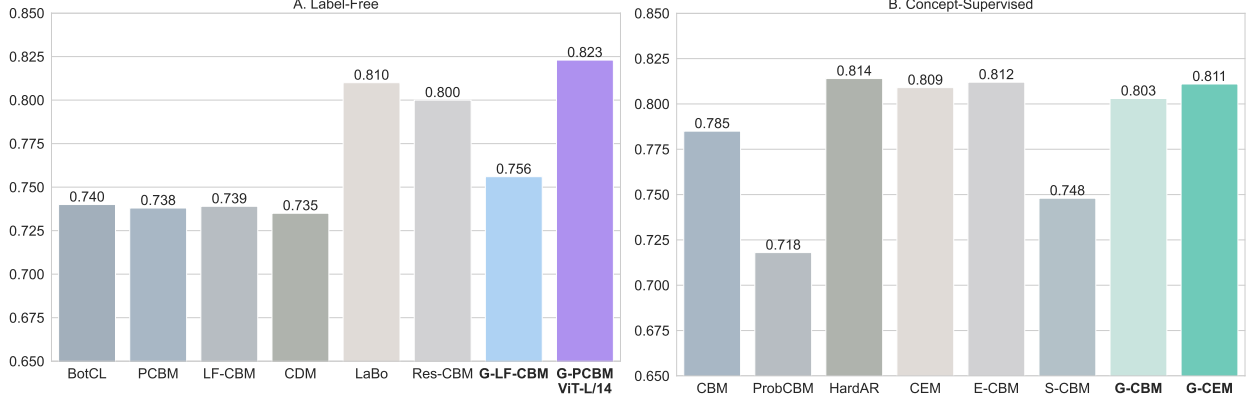


Figure 2: We compare our models with current SOTA results for corresponding training and dataset settings, i.e., label-free and concept-supervised. We report label accuracy in both subfigures.

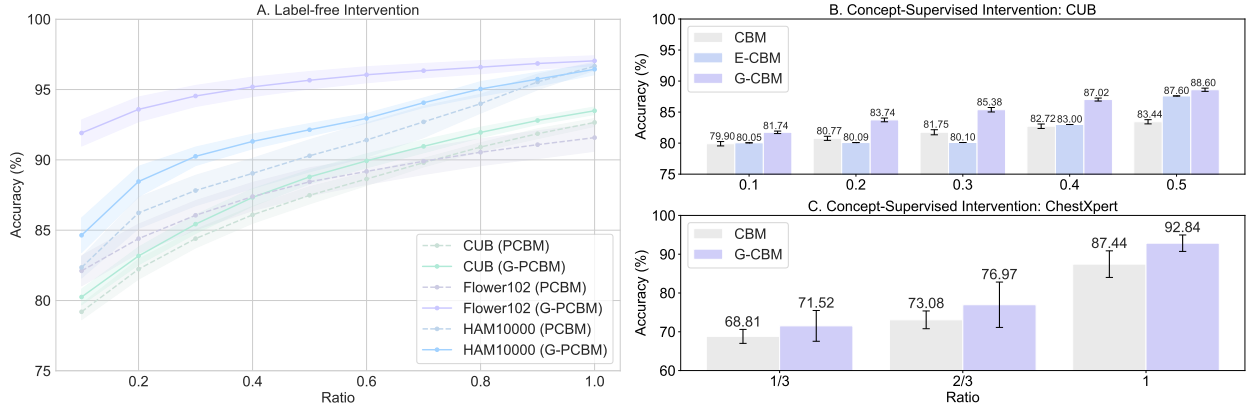


Figure 3: This figure shows the effectiveness of using latent graphs when intervening concepts. Subfigure A compares the after-intervention performance between PCBM and G-PCBM across three datasets under the label-free setting; subfigures B and C select concept-supervised datasets. Full ratio intervention comparisons between G-CBM and E-CBM are in appendix J.

In the concept-supervised setting (Figure 3 B & C), we compare performance on the CUB and ChestXpert datasets. Unlike E-CBM [19], which requires iterative energy calculations and gradients for intervention, G-CBM achieves strong results via a single forward pass. This efficiency, combined with high accuracy, highlights the benefit of explicitly modeling concept relations. We hypothesize that concept supervision encourages meaningful correlations, which the latent graph further captures and utilizes during intervention. The improved performance across datasets supports the positive impact of latent structure in enhancing interpretability and trust.

#### 4.5 How Contrastive Terms Affect Model Performance

**Using both  $\mathcal{L}_{emb}$  and  $\mathcal{L}_{act}$  is crucial for Graph LF-CBM.** Table 3 examines different combinations of contrastive losses on the CUB dataset. We find that using only  $\mathcal{L}_{emb}$  marginally improves performance, while incorporating  $\mathcal{L}_{act}$  leads to further gains. However, on HAM10000 and CIFAR-100, applying either loss alone fails to outperform the LF-CBM baseline. Notably, using both  $\mathcal{L}_{emb}$  and  $\mathcal{L}_{act}$  consistently achieves the best accuracy across tasks. When only  $\mathcal{L}_{emb}$  is used, the learned graph becomes overly dense due to insensitivity to the  $\ell_1$  regularization on edge weights. Conversely, relying solely on  $\mathcal{L}_{act}$  tends to yield overly sparse graphs. Thus, combining both objectives enables effective control of graph complexity and improves representation quality.

**With target supervision, contrastive regularization further enhances the expressivity of Graph PCBM.** Contrastive learning provides a self-supervised signal by treating concepts as alternative views of the same input. We investigate whether contrastive regularization still benefits Graph PCBM under target supervision. As shown in Table 4, applying both  $\mathcal{L}_{emb}$  and  $\mathcal{L}_{act}$  improves performance across CUB, HAM10000, and CIFAR-100. On CIFAR-100 in particular,

Dataset	CUB				HAM10000			
$\mathcal{L}_{emb}$	-	-	✓	✓	-	-	✓	✓
$\mathcal{L}_{act}$	-	✓	-	✓	-	✓	-	✓
Performance	73.90%	75.38%	74.11%	<b>75.59%</b>	66.76%	62.87%	65.10%	<b>67.47%</b>
Dataset	Flower102				CIFAR100			
$\mathcal{L}_{emb}$	-	-	✓	✓	-	-	✓	✓
$\mathcal{L}_{act}$	-	✓	-	✓	-	✓	-	✓
Performance	84.77%	76.78%	85.99%	<b>86.00%</b>	65.16%	62.97%	59.49%	<b>65.96%</b>

Table 3: Multi-level contrastive learning is crucial for self-supervised concept graph qualities. If we train Graph LF-CBMs with one excluding contrast loss, the model can fail to yield a good latent structure; while considering both contrast losses, models can gain more benefits.

Method (Graph PCBM)	CUB	HAM10000	CIFAR-100
w/o ( $\mathcal{L}_{emb} + \mathcal{L}_{act}$ )	76.89% ( $\pm 0.65\%$ )	77.66% ( $\pm 0.41\%$ )	75.67% ( $\pm 0.35\%$ )
w ( $\mathcal{L}_{emb} + \mathcal{L}_{act}$ )	<b>77.14%</b> ( $\pm 0.40\%$ )	<b>78.50%</b> ( $\pm 0.52\%$ )	<b>80.86%</b> ( $\pm 0.26\%$ )

Table 4: Adding contrast loss to target supervision can help model performance. Having the two contrast regularizers will lead to higher accuracy for label prediction.

we observe a performance gain of over 5%. Without contrast losses, the model relies entirely on target supervision and  $\ell_1$  regularization, making the learned graph highly sensitive to task-specific supervision signals and regularization strength. Contrast regularization thus provides a stable, auxiliary training signal that improves generalization and structure learning.

#### 4.6 How to Interpret The Concept Graph

**Latent graph can perform comparably to or recover a ground-truth concept graph in both settings.** We use ChatGPT [50] to generate 50 highly correlated concept pairs to build a "real-world" concept graph for *label-free* setting. Substituting the learned graph with this LLM-derived structure yields a CUB accuracy of **77.69%**, while our learnable graph achieves **77.14%**, demonstrating similar efficacy. Interestingly, LLMs excel at capturing surface-level similarities (e.g., color or body parts), while our method also discovers non-obvious correlations (e.g., "a loud, harsh cry" – "a raucous call"). In Figure 4, we also observe that concepts sharing the same label tend to be connected, regardless of architecture, validating that learned graphs reflect semantically meaningful groupings. In Appendix I, we can further extract salient subgraphs with fewer edges that maintain (or even improve) label accuracy and interpretability. Figures 9 & 10 show that key concept relations are retained, reinforcing the utility of our latent graph formulation. Interestingly, **latent graphs behave distinctly to different training regimes.** As shown in Figure 12, label-free models learn sparser graphs, while concept-supervised ones favor denser connections. More analyses are in Appendix K.

**Latent graphs improve robustness under concept attacks.** We conduct an experiment on the CUB dataset in Appendix F where we randomly mask or perturb a fixed number of concepts in three different groups: (1) connected concepts, (2) isolated concepts, and (3) random selections from the entire concept set. As shown in Figure 6, corrupting connected concepts results in significantly less performance degradation compared to isolated or randomly selected ones. This suggests that the latent graph enables the model to recover corrupted concept information by aggregating signals from clean neighboring nodes, thereby enhancing resilience against noise or missing data.

## 5 Limitations & Conclusions

Graph CBMs currently capture only latent concept interactions, without modeling hierarchies or complex relationships. Incorporating external knowledge about concept hierarchy could enhance interpretability, and future work will explore hierarchical structures beyond pairwise interactions.

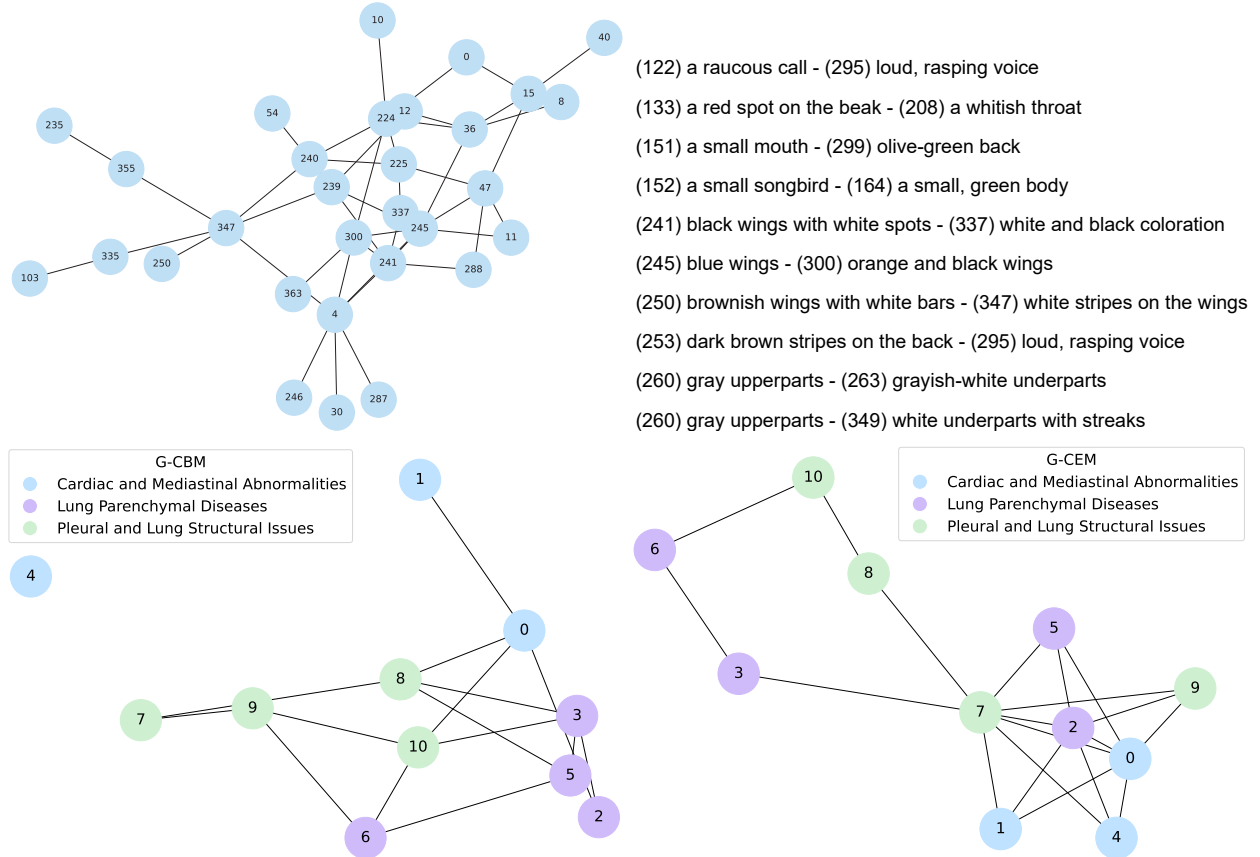


Figure 4: *Top*: Illustrating part of the learned latent graph under the label-free setting on CUB, alongside representative connected concept pairs. *Bottom*: G-CBM and G-CEM capture similar and trustworthy concept interactions for the ChestXpert dataset.

In this paper, we introduced Graph CBMs, a simple yet effective framework that incorporates graph structures to model concept correlations and enhance interpretability. Our method is orthogonal to existing CBMs and can be seamlessly integrated to boost performance while supporting targeted concept interventions. Notably, the learned latent graphs can match the effectiveness of ground-truth concept graphs. Future directions include leveraging external knowledge graphs for graph distribution modeling and extending latent graph techniques to interpret individual neurons within CBMs [51].

## References

- [1] Kaiming He, Xiangyu Zhang, Shaoqing Ren, and Jian Sun. Deep residual learning for image recognition. In *Proceedings of the IEEE conference on computer vision and pattern recognition*, pages 770–778, 2016.
- [2] Alexey Dosovitskiy, Lucas Beyer, Alexander Kolesnikov, Dirk Weissenborn, Xiaohua Zhai, Thomas Unterthiner, Mostafa Dehghani, Matthias Minderer, Georg Heigold, Sylvain Gelly, Jakob Uszkoreit, and Neil Houlsby. An image is worth 16x16 words: Transformers for image recognition at scale. In *International Conference on Learning Representations*, 2021.
- [3] Ilya O Tolstikhin, Neil Houlsby, Alexander Kolesnikov, Lucas Beyer, Xiaohua Zhai, Thomas Unterthiner, Jessica Yung, Andreas Steiner, Daniel Keysers, Jakob Uszkoreit, et al. Mlp-mixer: An all-mlp architecture for vision. *Advances in neural information processing systems*, 34:24261–24272, 2021.
- [4] Ashish Vaswani, Noam Shazeer, Niki Parmar, Jakob Uszkoreit, Llion Jones, Aidan N Gomez, Łukasz Kaiser, and Illia Polosukhin. Attention is all you need. *Advances in neural information processing systems*, 30, 2017.
- [5] Jacob Devlin, Ming-Wei Chang, Kenton Lee, and Kristina Toutanova. BERT: Pre-training of deep bidirectional transformers for language understanding. In Jill Burstein, Christy Doran, and Tamar Solorio, editors, *Proceedings of the 2019 Conference of the North American Chapter of the Association for Computational Linguistics: Human*

- Language Technologies, Volume 1 (Long and Short Papers)*, pages 4171–4186, Minneapolis, Minnesota, June 2019. Association for Computational Linguistics.
- [6] Tom Brown, Benjamin Mann, Nick Ryder, Melanie Subbiah, Jared D Kaplan, Prafulla Dhariwal, Arvind Nee-lakantan, Pranav Shyam, Girish Sastry, Amanda Askell, et al. Language models are few-shot learners. *Advances in neural information processing systems*, 33:1877–1901, 2020.
  - [7] Colin Raffel, Noam Shazeer, Adam Roberts, Katherine Lee, Sharan Narang, Michael Matena, Yanqi Zhou, Wei Li, and Peter J Liu. Exploring the limits of transfer learning with a unified text-to-text transformer. *Journal of machine learning research*, 21(140):1–67, 2020.
  - [8] Thomas N. Kipf and Max Welling. Semi-supervised classification with graph convolutional networks. In *International Conference on Learning Representations*, 2017.
  - [9] Yuning You, Tianlong Chen, Yongduo Sui, Ting Chen, Zhangyang Wang, and Yang Shen. Graph contrastive learning with augmentations. *Advances in neural information processing systems*, 33:5812–5823, 2020.
  - [10] Yu Rong, Tingyang Xu, Junzhou Huang, Wenbing Huang, Hong Cheng, Yao Ma, Yiqi Wang, Tyler Derr, Lingfei Wu, and Tengfei Ma. Deep graph learning: Foundations, advances and applications. In *Proceedings of the 26th ACM SIGKDD international conference on knowledge discovery & data mining*, pages 3555–3556, 2020.
  - [11] Pang Wei Koh, Thao Nguyen, Yew Siang Tang, Stephen Mussmann, Emma Pierson, Been Kim, and Percy Liang. Concept bottleneck models. In *International conference on machine learning*, pages 5338–5348. PMLR, 2020.
  - [12] Zoe Kourtzi and Charles E Connor. Neural representations for object perception: structure, category, and adaptive coding. *Annual review of neuroscience*, 34(1):45–67, 2011.
  - [13] Mateo Espinosa Zarlenga, Pietro Barbiero, Gabriele Ciravegna, Giuseppe Marra, Francesco Giannini, Michelangelo Diligenti, Zohreh Shams, Frederic Precioso, Stefano Melacci, Adrian Weller, Pietro Lio, and Mateja Jamnik. Concept embedding models: Beyond the accuracy-explainability trade-off. *Advances in Neural Information Processing Systems*, 35, 2022.
  - [14] Eunji Kim, Dahuin Jung, Sangha Park, Siwon Kim, and Sungroh Yoon. Probabilistic concept bottleneck models. *International conference on machine learning*, 2023.
  - [15] Mert Yuksekgonul, Maggie Wang, and James Zou. Post-hoc concept bottleneck models. In *The Eleventh International Conference on Learning Representations*, 2023.
  - [16] Moshe Bar. Visual objects in context. *Nature Reviews Neuroscience*, 5(8):617–629, 2004.
  - [17] Aude Oliva and Antonio Torralba. The role of context in object recognition. *Trends in cognitive sciences*, 11(12):520–527, 2007.
  - [18] Marton Havasi, Sonali Parbhoo, and Finale Doshi-Velez. Addressing leakage in concept bottleneck models. *Advances in Neural Information Processing Systems*, 35:23386–23397, 2022.
  - [19] Xinyue Xu, Yi Qin, Lu Mi, Hao Wang, and Xiaomeng Li. Energy-based concept bottleneck models: Unifying prediction, concept intervention, and probabilistic interpretations. In *The Twelfth International Conference on Learning Representations*, 2024.
  - [20] Tuomas Oikarinen, Subhro Das, Lam M. Nguyen, and Tsui-Wei Weng. Label-free concept bottleneck models. In *The Eleventh International Conference on Learning Representations*, 2023.
  - [21] Yue Yang, Artemis Panagopoulou, Shenghao Zhou, Daniel Jin, Chris Callison-Burch, and Mark Yatskar. Language in a bottle: Language model guided concept bottlenecks for interpretable image classification. In *Proceedings of the IEEE/CVF Conference on Computer Vision and Pattern Recognition*, pages 19187–19197, 2023.
  - [22] An Yan, Yu Wang, Yiwu Zhong, Chengyu Dong, Zexue He, Yujie Lu, William Yang Wang, Jingbo Shang, and Julian McAuley. Learning concise and descriptive attributes for visual recognition. In *Proceedings of the IEEE/CVF International Conference on Computer Vision (ICCV)*, pages 3090–3100, October 2023.
  - [23] Xiaowen Dong, Dorina Thanou, Michael Rabbat, and Pascal Frossard. Learning graphs from data: A signal representation perspective. *IEEE Signal Processing Magazine*, 36(3):44–63, 2019.
  - [24] Yue Yu, Jie Chen, Tian Gao, and Mo Yu. DAG-GNN: DAG structure learning with graph neural networks. In Kamalika Chaudhuri and Ruslan Salakhutdinov, editors, *Proceedings of the 36th International Conference on Machine Learning*, volume 97 of *Proceedings of Machine Learning Research*, pages 7154–7163. PMLR, 09–15 Jun 2019.
  - [25] Luca Franceschi, Mathias Niepert, Massimiliano Pontil, and Xiao He. Learning discrete structures for graph neural networks. In *International conference on machine learning*, pages 1972–1982. PMLR, 2019.

- [26] Thomas Kipf, Ethan Fetaya, Kuan-Chieh Wang, Max Welling, and Richard Zemel. Neural relational inference for interacting systems. In *International conference on machine learning*, pages 2688–2697. PMLR, 2018.
- [27] Chao Shang, Jie Chen, and Jinbo Bi. Discrete graph structure learning for forecasting multiple time series. In *International Conference on Learning Representations*, 2020.
- [28] Anees Kazi, Luca Cosmo, Seyed-Ahmad Ahmadi, Nassir Navab, and Michael M Bronstein. Differentiable graph module (dgm) for graph convolutional networks. *IEEE Transactions on Pattern Analysis and Machine Intelligence*, 45(2):1606–1617, 2022.
- [29] Tengfei Ma, Trong Nghia Hoang, and Jie Chen. Federated learning of models pre-trained on different features with consensus graphs. In *Uncertainty in Artificial Intelligence*, pages 1336–1346. PMLR, 2023.
- [30] Tianxin Wei, Yuning You, Tianlong Chen, Yang Shen, Jingrui He, and Zhangyang Wang. Augmentations in hypergraph contrastive learning: Fabricated and generative. In S. Koyejo, S. Mohamed, A. Agarwal, D. Belgrave, K. Cho, and A. Oh, editors, *Advances in Neural Information Processing Systems*, volume 35, pages 1909–1922. Curran Associates, Inc., 2022.
- [31] Ting Chen, Simon Kornblith, Mohammad Norouzi, and Geoffrey Hinton. A simple framework for contrastive learning of visual representations. In *International conference on machine learning*, pages 1597–1607. PMLR, 2020.
- [32] Leonardo FR Ribeiro, Pedro HP Saverese, and Daniel R Figueiredo. struc2vec: Learning node representations from structural identity. In *Proceedings of the 23rd ACM SIGKDD international conference on knowledge discovery and data mining*, pages 385–394, 2017.
- [33] Fan-Yun Sun, Jordan Hoffman, Vikas Verma, and Jian Tang. Infograph: Unsupervised and semi-supervised graph-level representation learning via mutual information maximization. In *International Conference on Learning Representations*, 2019.
- [34] Yuning You, Tianlong Chen, Yongduo Sui, Ting Chen, Zhangyang Wang, and Yang Shen. Graph contrastive learning with augmentations. In H. Larochelle, M. Ranzato, R. Hadsell, M. F. Balcan, and H. Lin, editors, *Advances in Neural Information Processing Systems*, volume 33, pages 5812–5823. Curran Associates, Inc., 2020.
- [35] Ziyang Wang, Huoyu Liu, Wei Wei, Yue Hu, Xian-Ling Mao, Shaojian He, Rui Fang, and Dangyang Chen. Multi-level contrastive learning framework for sequential recommendation. In *Proceedings of the 31st ACM International Conference on Information & Knowledge Management, CIKM '22*, page 2098–2107, New York, NY, USA, 2022. Association for Computing Machinery.
- [36] Tongzhou Wang and Phillip Isola. Understanding contrastive representation learning through alignment and uniformity on the hypersphere. In *International conference on machine learning*, pages 9929–9939. PMLR, 2020.
- [37] C. Wah, S. Branson, P. Welinder, P. Perona, and S. Belongie. The caltech-ucsd birds-200-2011 dataset. Technical Report CNS-TR-2011-001, California Institute of Technology, 2011.
- [38] Maria-Elena Nilsback and Andrew Zisserman. Automated flower classification over a large number of classes. In *Indian Conference on Computer Vision, Graphics and Image Processing*, Dec 2008.
- [39] Yongqin Xian, Christoph H Lampert, Bernt Schiele, and Zeynep Akata. Zero-shot learning—a comprehensive evaluation of the good, the bad and the ugly. *IEEE transactions on pattern analysis and machine intelligence*, 41(9):2251–2265, 2018.
- [40] Alex Krizhevsky, Geoffrey Hinton, et al. Learning multiple layers of features from tiny images. 2009.
- [41] Philipp Tschandl. The HAM10000 dataset, a large collection of multi-source dermatoscopic images of common pigmented skin lesions, 2018.
- [42] Jeremy Irvin, Pranav Rajpurkar, Michael Ko, Yifan Yu, Silviana Ciurea-Ilcus, Chris Chute, Henrik Marklund, Behzad Haghighi, Robyn Ball, Katie Shpanskaya, et al. Chexpert: A large chest radiograph dataset with uncertainty labels and expert comparison. In *Proceedings of the AAAI conference on artificial intelligence*, volume 33, pages 590–597, 2019.
- [43] Alec Radford, Jong Wook Kim, Chris Hallacy, Aditya Ramesh, Gabriel Goh, Sandhini Agarwal, Girish Sastry, Amanda Askell, Pamela Mishkin, Jack Clark, Gretchen Krueger, and Ilya Sutskever. Learning transferable visual models from natural language supervision. In Marina Meila and Tong Zhang, editors, *Proceedings of the 38th International Conference on Machine Learning*, volume 139 of *Proceedings of Machine Learning Research*, pages 8748–8763. PMLR, 18–24 Jul 2021.
- [44] Shruthi Bannur, Stephanie Hyland, Qianchu Liu, Fernando Perez-Garcia, Maximilian Ilse, Daniel C Castro, Benedikt Boecking, Harshita Sharma, Kenza Bouzid, Anja Thieme, et al. Learning to exploit temporal structure for biomedical vision-language processing. In *Proceedings of the IEEE/CVF Conference on Computer Vision and Pattern Recognition*, pages 15016–15027, 2023.

- [45] Bowen Wang, Liangzhi Li, Yuta Nakashima, and Hajime Nagahara. Learning bottleneck concepts in image classification. In *Proceedings of the IEEE/CVF conference on computer vision and pattern recognition*, pages 10962–10971, 2023.
- [46] Konstantinos P. Panousis, Dino Ienco, and Diego Marcos. Sparse linear concept discovery models. In *2023 IEEE/CVF International Conference on Computer Vision Workshops (ICCVW)*, pages 2759–2763, 2023.
- [47] Chenming Shang, Shiji Zhou, Hengyuan Zhang, Xinzhe Ni, Yujiu Yang, and Yuwang Wang. Incremental residual concept bottleneck models. In *Proceedings of the IEEE/CVF Conference on Computer Vision and Pattern Recognition (CVPR)*, pages 11030–11040, June 2024.
- [48] Moritz Vandenhirtz, Sonia Laguna, Ričards Marcinkevičs, and Julia E Vogt. Stochastic concept bottleneck models. In *Thirty-eighth Conference on Neural Information Processing Systems*, 2024.
- [49] Sungbin Shin, Yohan Jo, Sungsoo Ahn, and Namhoon Lee. A closer look at the intervention procedure of concept bottleneck models. In Andreas Krause, Emma Brunskill, Kyunghyun Cho, Barbara Engelhardt, Sivan Sabato, and Jonathan Scarlett, editors, *Proceedings of the 40th International Conference on Machine Learning*, volume 202 of *Proceedings of Machine Learning Research*, pages 31504–31520. PMLR, 23–29 Jul 2023.
- [50] Long Ouyang, Jeffrey Wu, Xu Jiang, Diogo Almeida, Carroll Wainwright, Pamela Mishkin, Chong Zhang, Sandhini Agarwal, Katarina Slama, Alex Ray, John Schulman, Jacob Hilton, Fraser Kelton, Luke Miller, Maddie Simens, Amanda Askell, Peter Welinder, Paul F Christiano, Jan Leike, and Ryan Lowe. Training language models to follow instructions with human feedback. In S. Koyejo, S. Mohamed, A. Agarwal, D. Belgrave, K. Cho, and A. Oh, editors, *Advances in Neural Information Processing Systems*, volume 35, pages 27730–27744. Curran Associates, Inc., 2022.
- [51] Tuomas Oikarinen and Tsui-Wei Weng. Linear explanations for individual neurons. In Ruslan Salakhutdinov, Zico Kolter, Katherine Heller, Adrian Weller, Nuria Oliver, Jonathan Scarlett, and Felix Berkenkamp, editors, *Proceedings of the 41st International Conference on Machine Learning*, volume 235 of *Proceedings of Machine Learning Research*, pages 38639–38662. PMLR, 21–27 Jul 2024.
- [52] TorchVision maintainers and contributors. Torchvision: Pytorch’s computer vision library. <https://github.com/pytorch/vision>, 2016.
- [53] Alejandro López-Cifuentes, Marcos Escudero-Viñolo, Jesús Bescós, and Álvaro García-Martín. Semantic-aware scene recognition. *Pattern Recognition*, page 107256, 2020.
- [54] Jia Deng, Wei Dong, Richard Socher, Li-Jia Li, Kai Li, and Li Fei-Fei. Imagenet: A large-scale hierarchical image database. In *2009 IEEE Conference on Computer Vision and Pattern Recognition*, pages 248–255, 2009.

## A Dataset Introduction

- Caltech-UCSD Birds-200-2011, CUB [37]: CUB is the most widely-used dataset for fine-grained visual categorization tasks. It contains 11,788 images of 200 subcategories belonging to birds, we follow the same data processing as done in the Label-free-CBM [20] setting to select 5,990 images for the training set and 5,790 images for the validation set. For the concept supervised setting, we process the same way as [11] and [13], selecting 112 attributes as the concepts and use the same data splits.
- Oxford 102 Flower [38]: is an image classification dataset comprising 102 flower categories. The flowers chosen to be flowers commonly occur in the United Kingdom. Each class consists of between 40 and 258 images. We follow the torchvision dataset setting [52] and only use the training set for training and the validation set for testing.
- CIFAR-10 & CIFAR-100 [40]: The CIFAR-10/100 dataset (Canadian Institute for Advanced Research, 10 classes) is a subset of the Tiny Images dataset and consists of 60,000 32x32 color images. CIFAR-10 labels images with one of 10 mutually exclusive classes, and CIFAR-100 has 100 classes grouped into 20 superclasses. There are 6000 images per class with 5000 training and 1000 testing images per class in CIFAR-10, while CIFAR-100 divides the dataset into 500 training images and 100 testing images per class.
- HAM10000 [41]: A dataset of 10000 training images for detecting pigmented skin lesions. It contains 7 labels and a representative collection of all important diagnostic categories in pigmented lesions HAM10000 provides 10,000 training images and 1,511 testing images.
- AwA2 [39] is a zero-shot learning dataset containing 37,322 images and 50 animal classes. Unlike the CUB dataset [37] in which concepts are defined at the instance level, images under the same label inside AwA2 [39] will share the same concepts. We use all 85 attributes as concepts.



- ChestXpert [42] is a large dataset of chest X-rays and competition for automated chest X-ray interpretation, consisting of 224,316 chest radiographs of 65,240 patients, which features 14 uncertainty observations and radiologist-labeled reference standard evaluation sets. ChestXpert [42] does not provide binary label classification, so we cluster 11 out of 14 observations into 3 categories. The detailed data processing can be found in appendix C.

The number of concepts for datasets is as follows: 370 for CUB, 108 for Flower, 48 for HAM10000, 30 for CIFAR-10, and 50 for CIFAR-100. For (G-)LF-CBM experiments, we use the original number concepts without any filtering (143 for CIFAR-10 & 892 for CIFAR-100).

## B Configuration and Running Environments

dataset	training epochs	Learning Rate	$\alpha$	$\beta$
CUB	100	1e-3	0.1	0.2
Flower102	500	1e-3	0.1	0.05
HAM10000	100	1e-3	0.1	0.05
CIFAR-10	100	1e-3	0.1	0.1
CIFAR-100	100	1e-3	0.1	0.05

Table 5: Training Configuration for Graph LF-CBM

dataset	training epochs	Learning Rate	$\alpha$	$\beta$
CUB	100	1e-3	0.1	0.2
Flower102	100	1e-3	0.1	0.01
HAM10000	100	1e-3	0.1	0.05
CIFAR-10	50	1e-3	0.1	0.05
CIFAR-100	30	1e-3	0.1	0.05

Table 6: Training Configuration for Graph PCBM

dataset	training epochs	Learning Rate	$\alpha$	$\beta$
CUB	100	1e-3	0.05	0.0
AwA2	50	1e-3	0.01	0.0
ChestXpert	50	1e-3	0.03	0.0

Table 7: Training Configuration for Graph CBM

dataset	training epochs	Learning Rate	$\alpha$	$\beta$
CUB	100	1e-3	0.07	0.0
AwA2	50	1e-3	0.07	0.0
ChestXpert	50	1e-3	0.07	0.0

Table 8: Training Configuration for Graph CEM

We run all the experiments on a single GPU (NVIDIA A100). The GPU memory for Graph LF-CBMs and Graph PCBMs is less than 10GB with a batch size of 512 for all datasets. The full training run takes from 3 minutes to 2.5 hours depending on the dataset size and the number of training epochs. In practice, Graph LF-CBMs trained on CIFAR-100 take 2.5 hours, while Graph PCBMs trained on Flower need less than 3 minutes for execution. Graph CBMs and Graph CEMs on average take 8~12 mins to finish training on the CUB and ChestXpert datasets, while they spend about 3~5 mins on the AWA2 dataset. We also offer time measurements in Table 9: since the latent graph introduces more computational units, the model will be unavoidable to spend more time on training.

## C Data Processing for ChestXpert

CheXpert [42] uses "No Finding" to indicate the abnormality of patients' chest radiographs, and it is highly unbalanced. We will then cluster CheXpert's concepts into 3 different labels, and we will use the frontal and lateral X-ray images for each patient. The concepts and labels are classified in this way:

Model	Training	Inference
PCBM	5.7it/s	2.09it/s
G-PCBM	9.43it/s	2.12it/s
CBM	6.12it/s	2.90it/s
G-CBM	7.89it/s	2.57it/s

Table 9: Time Measurement between our proposals and baselines

- **Group 1: Cardiac and Mediastinal Abnormalities:**

- Enlarged Cardiomeastinum
- Cardiomegaly
- Edema (related to heart conditions)

- **Group 2: Lung Parenchymal Diseases:**

- Lung Opacity
- Lung Lesion
- Consolidation
- Pneumonia

- **Group 3: Pleural and Lung Structural Issues:**

- Atelectasis (collapse of lung tissue)
- Pneumothorax (air in pleural space)
- Pleural Effusion
- Pleural Other

If one patient meets multiple abnormal conditions (multi-labeled), we will select the most significant abnormality. We choose not to include the *Fracture* observation, as it forms a cluster itself and shares no commonalities with other observations.

## D Lazy Intervention

**Lazy Intervention:** We define two sets of concept scores

$$\mathcal{R} = \{c_i \mid h(\tilde{c}_i) = y_i\}, \quad \mathcal{W} = \{c_i \mid h(\tilde{c}_i) \neq y_i\},$$

where  $\mathcal{R}$  and  $\mathcal{W}$  are sets of concept scores making right and wrong predictions. We can further partition them using class labels, so  $\mathcal{R} = \cup_{i=1}^m \mathcal{R}^i$ , and so does  $\mathcal{W}$ . We then define the difference set,

$$\mathcal{D} = \{\text{mean}(\mathcal{R}^j) - \text{mean}(\mathcal{W}^j) \mid 1 \leq j \leq m\},$$

$m$  is the number of classes. Each  $d^j \in \mathcal{D}$  can be viewed as a prototype of the intervention vector for  $j$ -th class. The intervention procedure will be

$$\text{Intervention} = \{c_i + d^j \mid \forall c_i \in \mathcal{W}^j, 1 \leq j \leq m\}.$$

When the dataset contains concept annotations, the  $\mathcal{R}$  records positively classified concepts, and the  $\mathcal{W}$  records falsely classified concepts. At the intervention step, *Lazy intervention* will only intervene on falsely classified concepts.

## E Having a Latent Concept Graph Enriches concept activations Expressivity

We want to understand the essential benefit brought by the latent graph when the model needs to make predictions. In order to offer a visualized explanation and evidence, we choose to draw the T-SNE plots for models trained on the Flower102 dataset (as this dataset contains sufficient many distinct labels and has a relatively balanced sample distribution). As shown in Figure 5, G-PCBM more likely admits isolated and independent concept score vector clusters, differentiating from PCBM which mixes some label groups spread up. Consequently, G-PCBM succeeds in gaining more expressivity for concept activations and boosting prediction performance substantially.

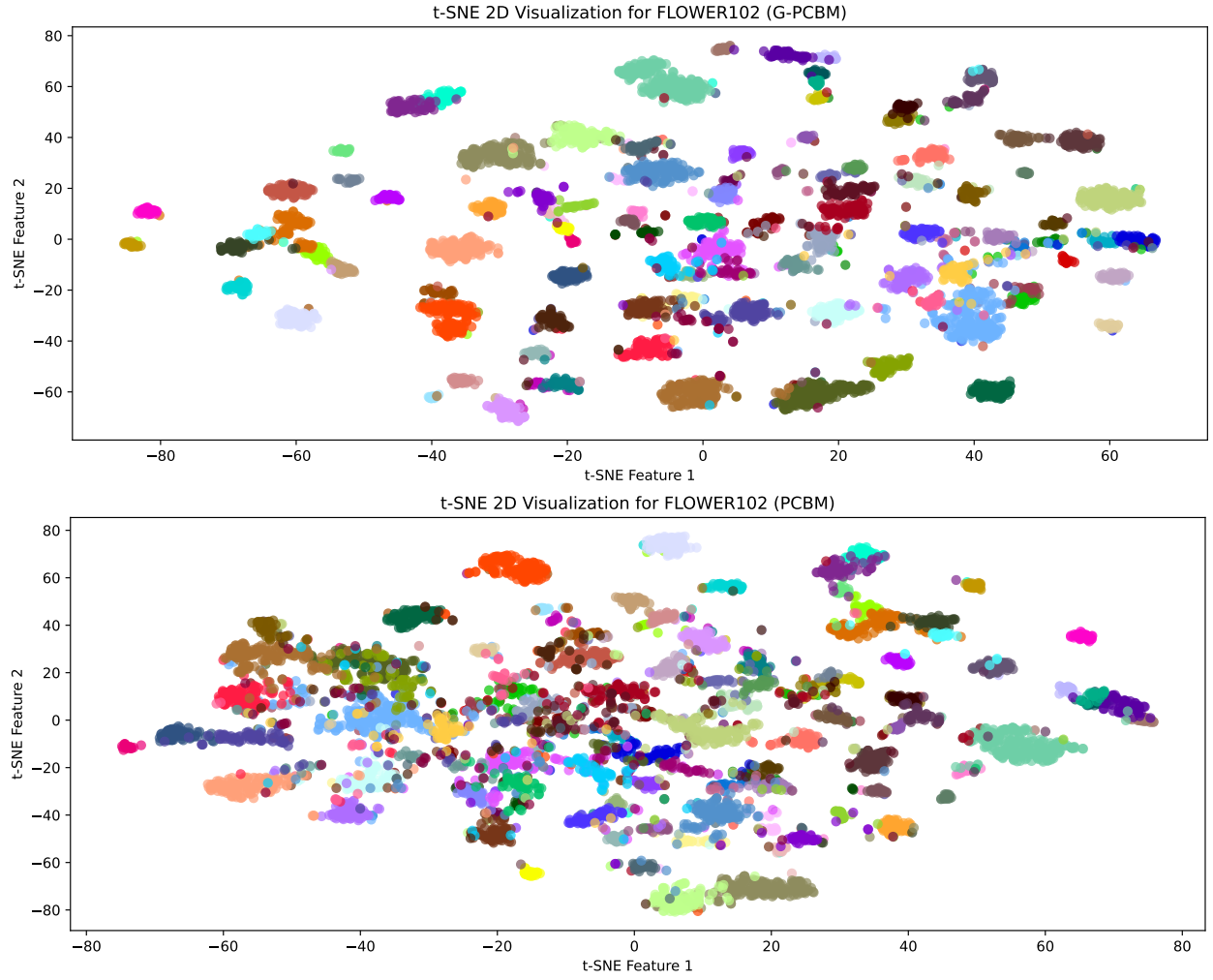


Figure 5: T-SNE visualization of concept activations distribution. *Top* shows a better clustering, while *bottom* has a more chaotic spread. Nodes with the same color are from the same label category.

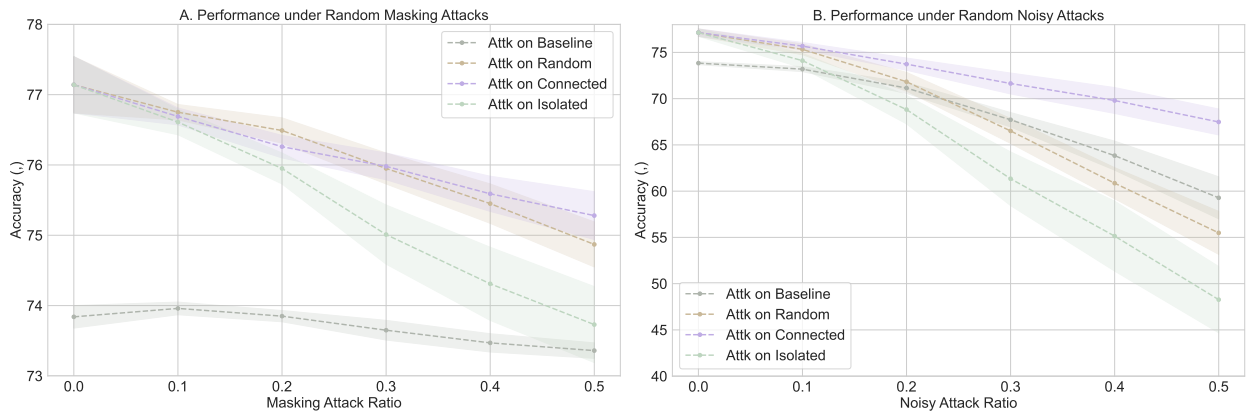


Figure 6: Attacking different types of concepts (nodes) in the CUB dataset can result in different scales of performance degradation.

## F Latent Graphs Offer Robustness under Label-Free Settings

In this section, we further investigate the effect of latent graphs on concepts (nodes), and we design a simple experiment to test such impacts. We first partition concepts into connected concepts (node degree  $\geq 1$ ) and isolated concepts, and we also keep the whole concept set as a baseline group for random attacks; then, we will randomly mask or perturb the same number of concepts in these groups separately; lastly, we let our model predict those corrupted concepts. We choose the CUB as the testing dataset for this experiment<sup>1</sup>.

As shown in Figure 6, attacking connected concepts does not harm the model performance as much as attacking isolated concepts or random concepts. We hypothesize that the latent graph structure provides much better robustness towards connected concepts, while the isolated ones cannot benefit from it. When masking or perturbing a concept, there will be information missing for the final prediction layer. Nevertheless, the latent graph structure can aggregate neighborhood information to recover the masked or perturbed concept so that the final prediction layer is still able to make a reasonable prediction.

## G Performance on other larger-scale datasets

Method	Places365			ImageNet		
	Acc	$\alpha$	$\beta$	Acc	$\alpha$	$\beta$
PCBM	55.16% ( $\pm 0.11\%$ )	-	-	77.49% ( $\pm 0.10\%$ )	-	-
Graph-PCBM	<b>55.25%</b> ( $\pm 0.08\%$ )	0.1	0.17	<b>78.48%</b> ( $\pm 0.10\%$ )	0.1	0.17

Table 10: We report the average accuracies from 4 different random seed experiments along with the standard deviation.

In this section, we investigate the performance enhancement in prediction and intervention brought by latent graphs on large-scale datasets. We choose *Places365* [53], a scene recognition dataset composed of 10 million images comprising 434 scene classes, and *ImageNet* [54] which contains 14,197,122 annotated images according to the WordNet hierarchy. We train G-PCBMs on these two datasets with 10 epochs, 1024 batch size, learning rate at 0.01, and Adam optimizer.

In Table 10, the G-PCBM has a latent graph to help capture the intrinsic concept correlation and improve label prediction in both large-scale datasets. We continue to present the positive impacts of involving a concept latent graph inside the model on *ImageNet* as a case study for intervention. Figure 7 also indicates the effectiveness of latent graphs in intervening large-scale datasets. In particular, G-PCBM significantly improves intervention performance in low intervention ratios. This also aligns with the results we conclude in the other datasets.

## H Latent Graphs Benefit Various CBM Backbones

In this section, we validate the effectiveness of the latent graph on other CBM backbones. We choose CDM [46] as the case study to show the benefits of latent graphs. The most important unit in CDM [46] is the concept presence indicator which is modeled from a Bernoulli distribution, and the motivation behind the indicator variable is to sparsify the required concepts for label prediction. In Figure 8, applying latent graph to CDM can make a great enhancement in terms of label prediction, and latent graph can help to recover those filtered concept information to further boost model performance. The phenomenon is similar to what we have discussed in F, as masking attacks also sparsify concepts, and the latent graph can prevent the degradation caused by such attacks or operations. Along with the performance enhancements in Tables 1 and 2, learning latent graphs offers a robust generalization ability across different model architectures and training settings, which encourages the expectation of latent graphs effectiveness on other methodologies like LaBo, HardAR, and E-CBM.

## I Salient Subgraph for Concept-Supervised Settings

The concept-supervised setting favors dense graphs, but it also easily leads to redundant connectivity for the latent graph, which will harm the concept graph interpretability and inference efficiency. We follow a heuristic strategy to find the salient subgraph inside the original concept graph: we mask one edge at a time and check the performance;

<sup>1</sup>We select checkpoints with a similar amount of connected concepts and isolated concepts.

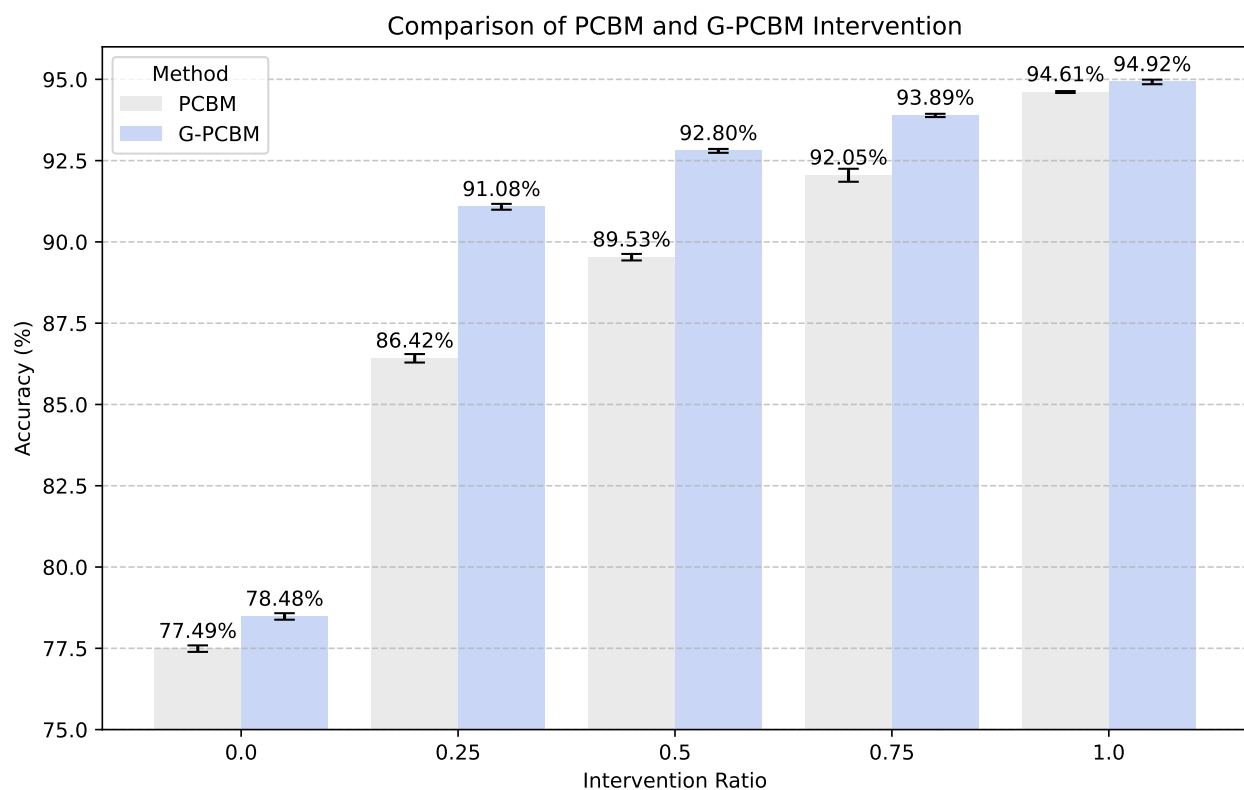


Figure 7: In a large-scale dataset, having latent graphs can still promote models to interact with intervention at different ratios.

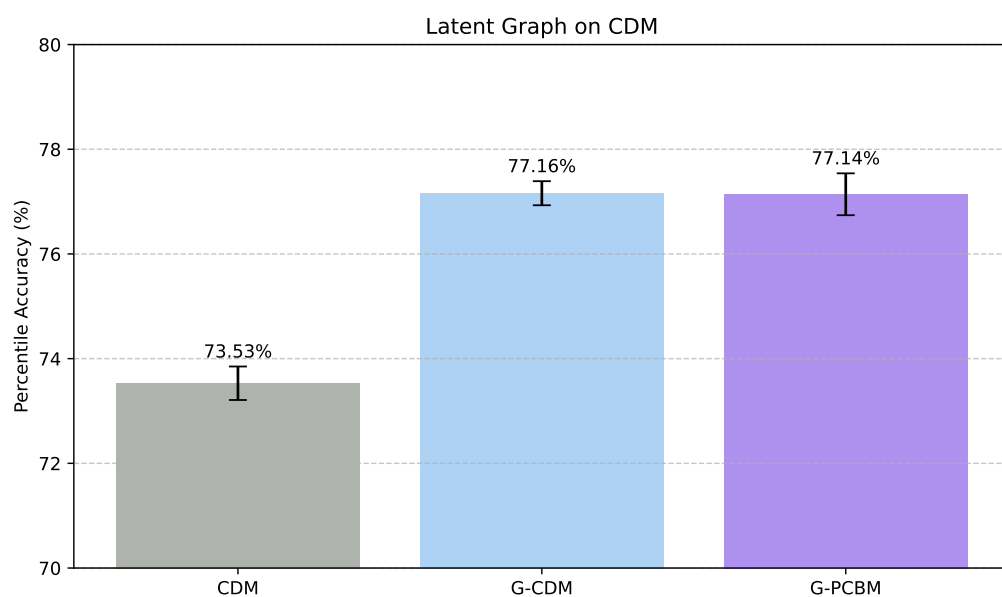


Figure 8: Adding a latent graph to the CDM can significantly improve model performance.

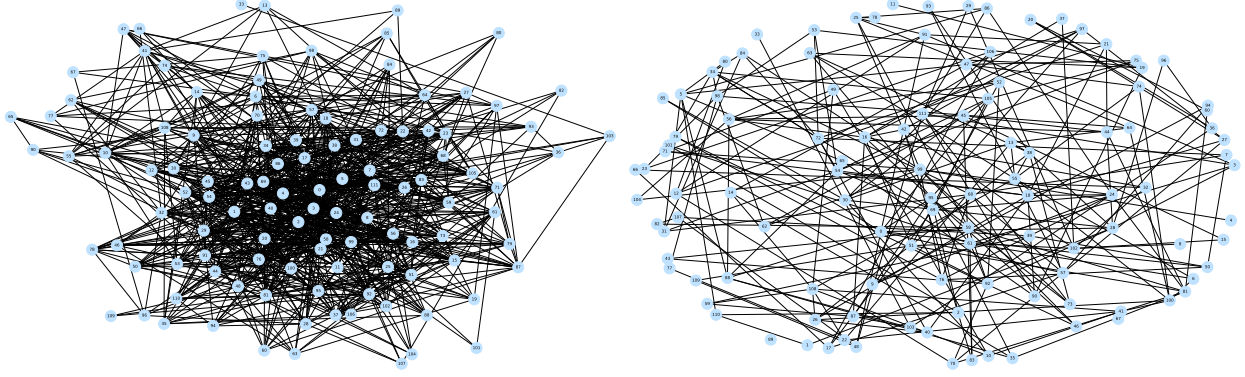


Figure 9: Both graphs are G-CBM concept graphs for the CUB dataset. Right: original concept graph. Left: salient subgraph structure.

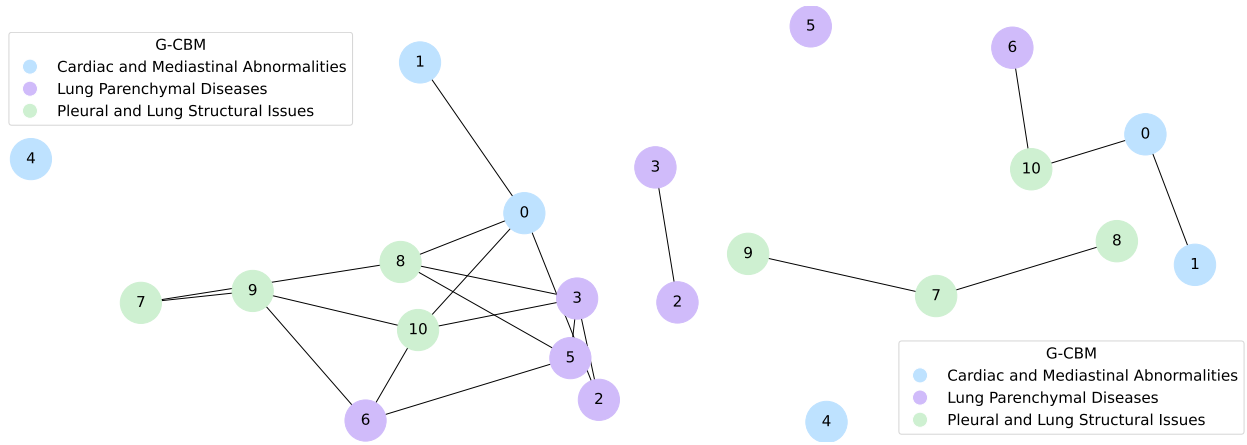


Figure 10: Both graphs are G-CBM concept graphs for the ChestXpert dataset. Right: original concept graph. Left: salient subgraph structure.

if the performance remains the same or goes up, we delete that edge from the original subgraph. By doing this, we can improve our label prediction marginally without sacrificing concept prediction (CUB label accuracy: 80.03% → **80.40%**; concept AUC: 83.20% → 83.20%; # of edges: 679 → **239**). Extracting the salient subgraph makes the concept graph more easily interpretable: for example in Figure 10, we can filter out the redundant edges and draw a more sparse concept graph. In the salient subgraph, concepts belonging to the same label class are more likely to connect. This also demonstrates that our latent graph effectively captures the hidden concept correlation embedded in the concept supervision.

We provide a quote from ChatGPT to show the reasonable connection between two node pairs: (node 6 (*Pneumonia*) and node 10 (*Pleural Other*)):

A. Pneumonia can directly affect the pleura, leading to conditions like pleural effusion, empyema, or pleurisy. These pleural complications often arise due to inflammation or infection spreading from the lungs to the pleural space, making the relationship between pneumonia and pleural disease significant in both diagnosis and treatment.

And (node 0 (Enlarged Cardiomeastinum), node 10 (Pleural Other)):

**Cardiac or vascular causes:** Enlarged cardiomeastinum often results from cardiac enlargement (e.g., heart failure or pericardial effusion) or vascular abnormalities (like aortic aneurysms). Some of these conditions can also cause pleural changes. For example:

1) Heart failure can lead to pleural effusion (fluid in the pleural space), which may manifest as a "Pleural Other" abnormality.

2) Aortic aneurysm or dissection may affect surrounding pleural structures due to proximity, causing pleural thickening or effusions.

**Malignancies:** Tumors in the mediastinum (e.g., lymphomas or metastatic disease) can enlarge the cardiomeastinum and simultaneously invade or affect the pleura, leading to pleural abnormalities.

**Infections and inflammatory conditions:** Severe infections like tuberculosis or mediastinitis can affect both the mediastinum and pleura, causing enlargement of the cardiomeastinum and pleural changes.

## J G-CBM Intervention at full ratio

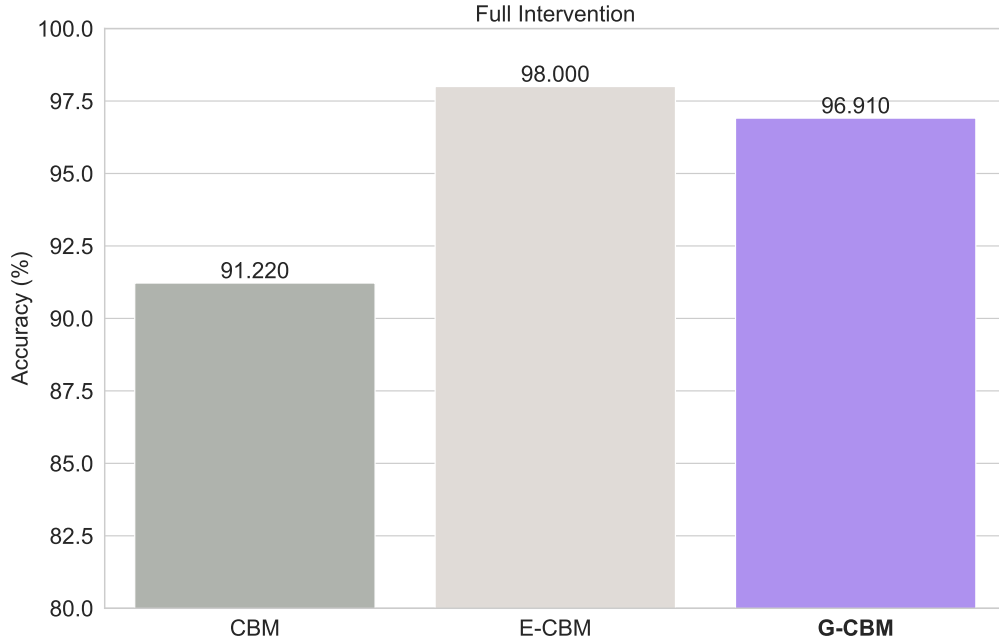


Figure 11: Comparison among models when full interventions.

We compare our G-CBMs with E-CBMs [19] and standard CBMs [11] at full interventions. In Figure 11, G-CBMs can improve the performance significantly compared to the standard CBMs, and it can match up with E-CBMs as well. E-CBMs require energy calculations and gradient backpropagations to update the label probability, so the full intervention can offer sufficient information for E-CBMs to reach a good after-intervention performance. However, E-CBMs cannot handle low-ratio intervention well as shown in Figure 3 B, while our G-CBMs can be effective at different intervention ratios coherently. Plus, one-step intervention makes G-CBMs more efficient.

## K Graph Complexity

**Graph CBMs favor sparse graphs under the label-free settings.** Without concept supervision, Graph CBMs prefer sparse graphs in general. As shown in Figure 12, the model gains performance improvement as we continue making the learnable graph sparse. Dense graphs result in over-smoothing concept scores, while sparse graphs can better preserve each concept value and propagate concept relation reasonably. We compare different graph complexity effects on the CUB dataset by varying the hyperparameter  $\beta$  (large  $\beta$  indicates more sparsity in the graph) under the Graph PCBM setting. We observe that our Graph PCBMs favor sparse graphs. The reason might be due to the way one collects concepts. If the model is trained under the label-free setting, one relies on a sophisticated concept generator like LLMs; however, LLMs will easily provide lots of redundant and repeated concepts. On the other hand, if the dataset contains concept annotations, concept sets are usually smaller in terms of the number of concepts and sufficiently informative. Moreover, concept annotations can act as an implicit concept correlation supervision, and models are expected to capture those hidden correlations in nature.

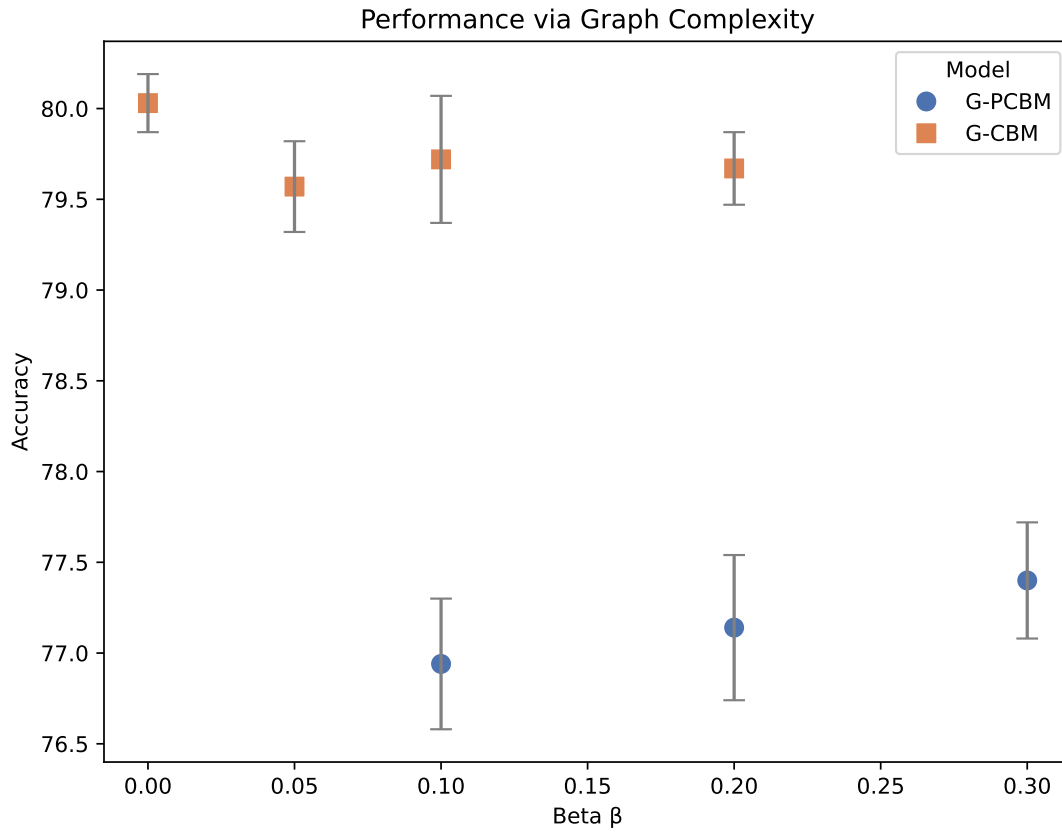


Figure 12: Performance changes as we set different  $\beta$  value to control the latent graph complexity.

## L Visualization of Learnable Graph





Figure 13: The overview of the CUB's concept graph in label-free settings.